DEUTSCHES ELEKTRONEN-SYNCHROTRON

DESY 94-023
February 1994

Exotic Particle Searches, Photoproduction and Diffraction in DIS at HERA

N. Harnew

Department of Physics, University of Oxford, UK

ISSN 0418-9833

NOTKESTRASSE 85 - 22603 HAMBURG

To be sure that your preprints are promptly included in the HIGH ENERGY PHYSICS INDEX, send them to (if possible by air mail):

DESY **Bibliothek** **Notkestraße 85** **22603 Hamburg** **Germany**	**DESY-IfH** **Bibliothek** **Platanenallee 6** **15738 Zeuthen** **Germany**

DESY 94-023
February 1994
ISSN 0418-9833

Exotic Particle Searches, Photoproduction and Diffraction in DIS at HERA

Neville Harnew *
Department of Physics, University of Oxford,
1 Keble Road, Oxford OX1 3RH, UK

A search has been made for leptoquarks, leptogluons and excited electrons for masses ranging from 35 to 250 GeV with the H1 and ZEUS detectors at HERA. No evidence for the production of such particles has been found in various decay channels and limits for the coupling strengths of such objects are derived. Soft and hard photoproduction processes are studied for γp centre of mass energies in the range W = 130 to 270 GeV and the γp total cross section is determined at a mean W of 200 GeV. Hard γp collisions with high p_T jets in the final state show inclusive jet and di-jet distributions which exhibit the characteristics expected for direct and resolved photon interactions. In deep inelastic, neutral current scattering at $\sqrt{s}$=296 GeV events are observed with a large rapidity gap in the hadronic final state. The underlying production mechanism of these events is interpreted as the diffractive dissociation of the virtual photon.

1. Introduction

This paper presents results obtained by the H1 and ZEUS collaborations, each using data corresponding to an integrated luminosity of approximately 25 nb^{-1} from collisions of 26.7 GeV electrons with 820 GeV protons at the HERA accelerator during the 1992 running period. The H1 and ZEUS experiments are multipurpose magnetic detectors, details of which are described elsewhere [1, 2]. During this running period of HERA only 9 out of 210 bunches were filled for collision in each of the electron and proton rings and the electron and proton beam currents were typically 10 mA. Additional single unpaired bunches of electrons and protons permitted a measurement of beam related backgrounds.

This paper summarizes the following results from the H1 and ZEUS experiments : a) the search for leptoquarks, leptogluons and excited electrons, b) soft and hard photoproduction including separating the direct and resolved photon processes and c) the observation of events with a large rapidity gap in deep inelastic scattering (DIS). A measurement of the F_2 structure function and an analysis of the hadronic final state in DIS events is described in a companion paper [3].

2. Exotic Particle Searches

In the Standard Model leptons and quarks interact only through electroweak forces. New lepton-quark forces predicted in many extensions of the Standard Model [4] could result in bound states of leptons and quarks, so-called leptoquark (LQ) states. Results from LEP [5] and Fermilab [6] give coupling-independent lower limits on their masses of 44 and 133 GeV, respectively. The latter limit assumes the most optimistic $LQ \rightarrow eq$ branching ratio (100%). In addition, leptogluons (LGs) are predicted in composite models where the weak gauge bosons and leptons are bound states of colour constituents [7].

* Invited talk given at the 9th Topical Workshop on Proton-Antiproton Collider Physics, Tsukuba, Japan, 18th-22nd October 1993, representing the H1 and ZEUS Collaborations.

Electron-proton collisions at HERA provide a natural and complementary search possibility. Here a leptoquark can be produced as a bound s-channel resonant state of electron and quark; a leptogluon as a bound state of lepton and gluon. Figure 1 shows the LQ and LG production and decay mechanisms. The predominant backgrounds, also shown in figure 1, are the deep inelastic scattering (DIS) processes. These have identical final state topologies: the neutral current (NC) process to the $LQ \rightarrow eq$ decay and the charged current (CC) process to the $LQ \rightarrow e\nu$ decay. The production of a LQ state will be signalled by a resonant peak in the effective mass of electron and quark jet, m_{eq}, or alternatively by a peak in the Bjorken x variable at $x_0 = \frac{m_{LQ}^2}{s}$, where s is the ep centre of mass energy squared. The total cross section for LQ production, assuming a small resonant width, ignoring radiative corrections and DIS/LQ interference is given by [8] $\sigma = \frac{\pi}{4s} g^2 u(x_0, Q^2)$ where $u(x_0, Q^2)$ is the probability density for finding the quark at $x = x_0$ and the four momentum transfer scale is taken to be $Q^2 = m_{LQ}^2$. The coupling constant $g = \sqrt{g_R^2 + g_L^2}$ is composed of left-handed (g_L) and right-handed (g_R) couplings at the electron-quark-leptoquark vertex. The $LQ \rightarrow eq$ decay mode is sensitive to g_L and g_R; however the pure left-handed current $LQ \rightarrow \nu q$ is sensitive only to g_L.

The NC background to LQ production is dominated by γ exchange and gives a rate proportional to $\frac{1}{Q^4}$. Conversely the scalar LQ (for example) has spin zero and hence has a uniform distribution in $\cos\theta^*$, where θ^* is the decay polar angle in the LQ rest frame. This is simply related to the scaling variable y by $1 - y = (1+\cos\theta^*)/2$, hence a suitable cut in y or alternatively $Q^2 (= sxy)$ will substantially reduce the background with respect to the signal.

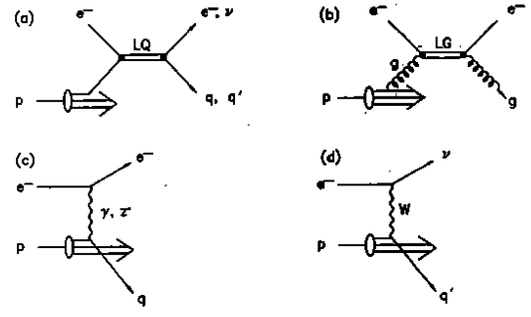

Figure 1: Production mechanisms for (a) leptoquark production, (b) leptogluon production, (c) DIS neutral current and (d) DIS charged current interactions.

Details of the H1 and ZEUS analyses can be found in references [9] and [10] respectively. The H1 electron-jet effective mass distribution, based on 25 nb^{-1} of data, is shown in figure 2, before and after the kinematic cut of $y > 0.25$ (chosen to optimize the signal to background ratio for the scalar LQ search). Shown for comparison is a DIS Monte Carlo simulation. Both the absolute number of events and the shape of the mass spectrum are well reproduced by the MC and no significant indication of a LQ resonance is observed. Rejection limits are derived for the hypothesis that all events are standard DIS background.

Assuming the absence of a signal, 95% confidence limits on g_L and g_R have been calculated as a function of m_{LQ} for the two experiments. For example, figure 3 shows the excluded regions of g_L (assuming g_R=0) for the S_0 leptoquark, measured by ZEUS. Quoted mass limits are determined assuming an electromagnetic coupling strength, ie $g_{L,R} = \sqrt{4\pi\alpha_{EM}} \simeq 0.31$. Table 1 gives the mass limits for generic leptoquark types; the notation is defined in reference [8]. The columns provide the charge (q), fermion number ($F = 3B + L$), weak isospin (I_{WK}) and flavour. It can be seen that mass limits for the scalar leptoquark currently approach 180 GeV assuming EM coupling. At full HERA luminosity the leptoquark search region will extend to the kinematic limit (296 GeV).

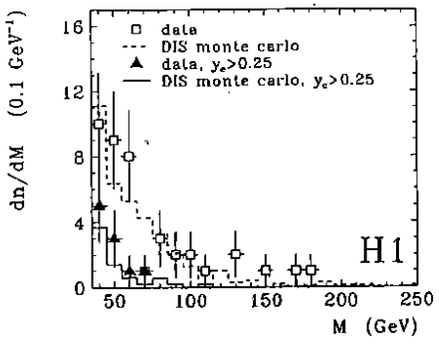

Figure 2: The H1 electron-jet mass spectrum above 35 GeV before and after the kinematic cut y >0.25. The histograms represent DIS Monte Carlo predictions.

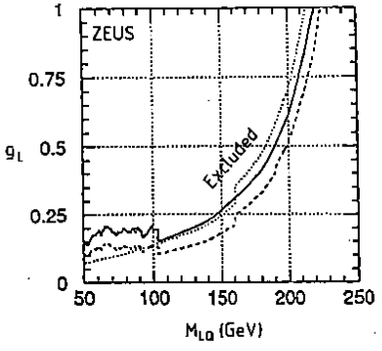

Figure 3: ZEUS 95% confidence limits for the exclusion of the S_0 leptoquark for its coupling g_L versus mass (assuming g_R=0) : from the CC sample (dotted line), from the NC sample (solid line) and from both (dashed line).

Using a similar analysis, 95% confidence limits can be placed on the mass of the spin $\frac{1}{2}$ leptogluon. In this case the cross section can be characterized by the formalism of reference [11], $\sigma_{LG} = \frac{2\pi^2}{4\alpha}\alpha_s(\frac{m_{LG}^2}{\Lambda})^2 G(x_0, Q^2)$ where $G(x_0, Q^2)$ is the probability of finding a gluon at $x = x_0$, α_s is the strong coupling constant and Λ is the characteristic mass scale. The Q^2 scale is taken to be m_{LG}^2. Figure 4 summarizes the excluded range in $\Lambda - m_{LG}$ space for H1 and table 2 gives specific exclusion values for both experiments.

The search for excited electrons (e^*) is an obvious field of interest in electron scattering experiments. They occur naturally in composite models [12] and if found would constitute strong evidence for a new layer of structure in the leptonic sector. The most stringent limits on their direct production come from LEP [13] where they can be pair or singly produced up to the Z^0 mass. At HERA e^*s can in principle be produced up to the kinematic limit of 296 GeV via the process $ep \to e^*X$, shown in figure 5. The decay mode $e^* \to e\gamma$ provides the most striking signature, however the high centre of mass energy also allows a search in

Leptoquark Species	q	F	I_{WK}	Mass limits (GeV) H1 L.H.	H1 R.H.	ZEUS L.H.	ZEUS R.H.
S_0	$-\frac{1}{3}$	−2	0	181	178	176	183
$\tilde{S}_0$	$-\frac{4}{3}$	−2	0	–	144	–	151
S_1	$-\frac{1}{3}, -\frac{4}{3}$	−2	1	192	–	188	–
$S_{\frac{1}{2}}$	$-\frac{2}{3}, -\frac{5}{3}$	0	$\frac{1}{2}$	98	112	93	117
$\tilde{S}_{\frac{1}{2}}$	$-\frac{5}{3}$	0	$\frac{1}{2}$	98	–	93	–
V_0	$-\frac{2}{3}$	−2	0	98	100	120	120
$\tilde{V}_0$	$-\frac{5}{3}$	−2	0	–	100	–	120
V_1	$-\frac{2}{3}, -\frac{5}{3}, -\frac{8}{3}$	−2	1	120	–	137	–
$V_{\frac{1}{2}}$	$-\frac{1}{3}, -\frac{4}{3}, -\frac{7}{3}$	0	$\frac{1}{2}$	151	190	173	207
$\tilde{V}_{\frac{1}{2}}$	$-\frac{4}{3}$	0	$\frac{1}{2}$	183	–	202	–

Table 1: Table of scalar (S) and vector (V) leptoquark properties and experimental mass limits, assuming EM coupling.

LG mass (GeV)	Λ scale (TeV) H1	ZEUS
100	1.8	1.3
200	0.20	0.15

Table 2: Table of leptogluon experimental mass limits.

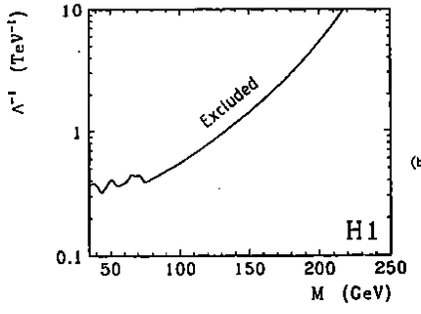

Figure 4: H1 95% rejection limits for the exclusion of the spin $\frac{1}{2}$ leptogluon as a function of inverse mass scale ($\frac{1}{\Lambda}$) and leptogluon mass.

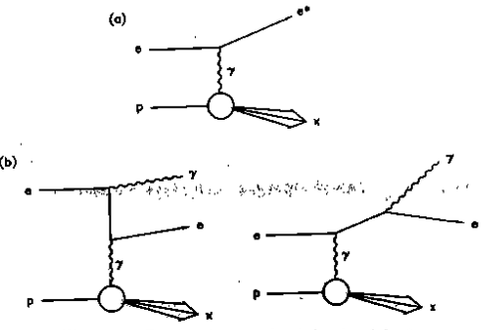

Figure 5: Production mechanisms for (a) e^* production and (b) QED Compton background processes.

the yet uninvestigated channels $e^* \to eZ^0$ and $e^* \to \nu W$. Both H1 and ZEUS have undertaken such a search [9, 14].

Backgrounds to the $e^* \to e\gamma$ search consist predominantly of wide-angle $e\gamma \to e\gamma$ Compton scattering, also shown in figure 5. These events are topologically similar to the $e^* \to e\gamma$ process but can be largely suppressed by a selection on the polar angle (θ) with respect to the proton beam of both e and γ electromagnetic showers. For example the ZEUS analysis requires two electromagnetic showers in the calorimeter with E_T >10 GeV (e^-) and > 2 GeV (γ) in addition to standard DIS cuts [14]. An additional cut on both calorimeter clusters of $\theta > 155^0$ reduces the Compton background by approximately 95% whilst retaining typically 70% of the e^* signal. Background from DIS events where a final state particle (eg a π^0) is misidentified as a γ is estimated to be negligible.

Figure 6(a) shows a Monte Carlo simulation of a 100 GeV e^* in the ZEUS detector and figure 6(b) shows the ZEUS selected data for the 25 nb^{-1} sample. A total of 7 events survive the cuts with no event having an $e\gamma$ effective mass greater than 20 GeV. The data agree in absolute magnitude and shape with expectations from the Compton simulation. Figure 7 shows one such Compton candidate recorded in the ZEUS detector. Given no candidate event, the experiments quote 95% confidence limits on coupling times branching ratio for the production of e^*s as a function of mass. The e^* is assumed to be a spin $\frac{1}{2}$ state which

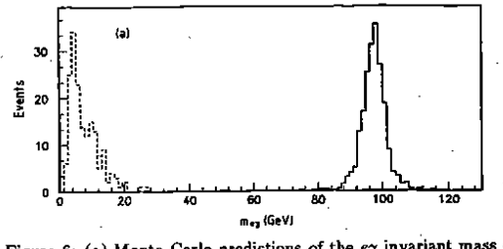

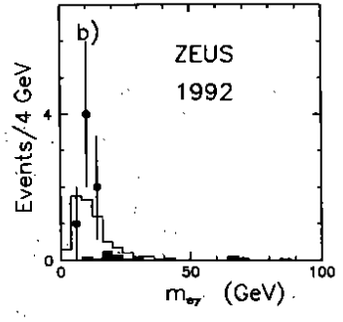

Figure 6: (a) Monte Carlo predictions of the $e\gamma$ invariant mass distribution for a 100 GeV e^* (solid line) and for the QED Compton process (dashed line) in the ZEUS detector and (b) the measured distribution (error bars) compared to the QED Monte Carlo (open histogram) and misidentified DIS (solid histogram).

has a magnetic-type coupling to standard leptons and bosons. Using the notation of Hagiwara et al [12], the e^* production cross section through t-channel photon exchange can be written in its most general form by $\sigma(ep \to e^*X) = \frac{|c|^2+|d|^2}{\Lambda^2}\sigma_0(m_{e^*})$ where Λ is a mass characterizing the compositeness scale and c and d are two coupling parameters. The quantity σ_0 is calculable and coupling independent, is a function of e^* mass and is the result of an integration over phase space and structure functions.

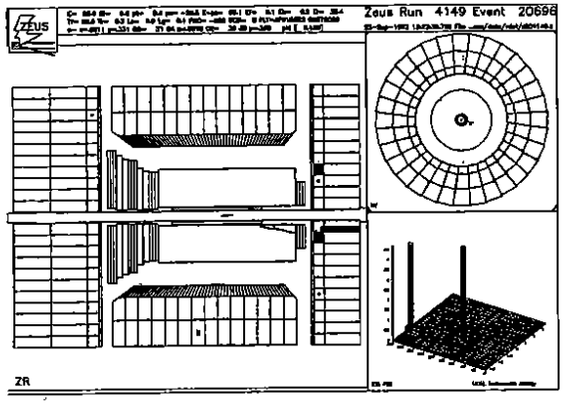

Figure 7: A QED Compton candidate observed in the ZEUS detector.

Figure 8 shows the 95% confidence level limits on the product of the coupling and branching ratio for each of the three possible e^* decay modes from the two experiments. Coupling dependent limits extend up to 225 GeV and even with limited luminosity, HERA already spans a search range beyond the reach of LEP. If indeed e^*s do not exist, the integrated luminosity accumulated in 1993 will bring HERA limits down at least a factor of four beyond what is quoted here.

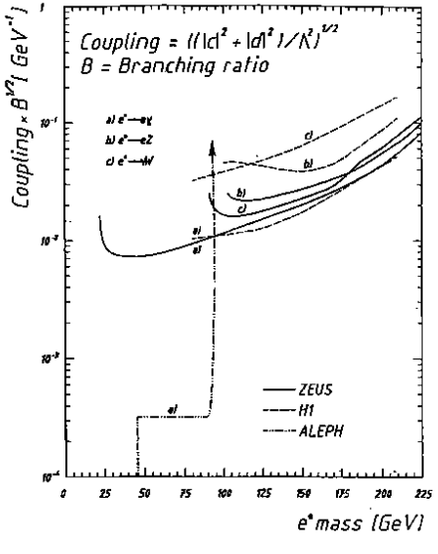

Figure 8: 95% rejection limits for e* production as a function of coupling constant and mass for ZEUS and H1.

3. Photoproduction

Neutral current ep interactions are described by the exchange of a neutral gauge vector boson. If the scattering angle of the electron is small then the four momentum transfer, Q^2, is small and the exchanged particle can be thought of as a quasi-real photon. In this way, ep interactions at small Q^2 can be used to measure the γp photoproduction process. Figure 9(a) shows the basic photoproduction mechanism together with a definition of the scattering parameters. Assuming the quasi-real photon to be collinear with the incident electron, it can be shown that the centre of mass energy in the γp rest frame is given by $W = \sqrt{ys}$ where y is the standard DIS scaling parameter discussed in section 2,

namely $y = \frac{E_e - E'_e}{E_e}$ where E_e and E'_e are the incident and scattered electron energies respectively. Hence HERA can be thought of as a γp collider; it is possible to measure values of W extending from approximately 10 GeV up to 296 GeV in a single experiment.

The photon is a very interesting particle. It is a point-like gauge boson which interacts with leptons and quarks via the EM interaction and also possesses a hadronic component in the form of quarks and gluons via internal virtual loops. The copious rate of γp interactions at HERA allows the quark and gluon components of the photon, ie F_2^γ, to be directly studied.

The H1 and ZEUS luminosity monitors are crucial components in the analysis of photoproduction events. These are comprised of downstream counters at small angles which independently tag the γ and scattered electron from the bremsstrahlung process $ep \to e'\gamma p$ in order to make the luminosity measurement [1, 2]. The scattered electron in photoproduction events will in some cases be detected in the luminosity electron counter for Q^2 below $\sim 2 \times 10^{-2}$ GeV^2. Events are thus referred to as 'tagged' or 'untagged' depending on whether this electron measurement is made.

The total photoproduction cross section can be decomposed into a set of different subprocesses, namely $\sigma_{tot}^{\gamma p} = \sigma_{soft}^{\gamma p} + \sigma_{resolved}^{\gamma p} + \sigma_{direct}^{\gamma p}$. The quantity $\sigma_{soft}^{\gamma p}$ is the diffractive component of the scattering process and contains contributions from 'elastic' vector dominance (VDM) giving $\gamma p \to Vp$ where V is a vector meson such as the ρ^0, single diffractive dissociation $\gamma p \to Xp$ or VX and double diffractive dissociation $\gamma p \to XX'$. The VDM diffractive component is shown schematically in figure 9(b) and involves virtual Pomeron-like exchange. The second term, $\sigma_{resolved}^{\gamma p}$, is the so-called 'resolved photon' component of the cross section. This term reflects the hadronic nature of the photon and involves hard VDM and inelastic processes, examples of which are shown in figure 9(c). Here a parton in the proton is scattering from a hadronic parton in the photon, typically giving rise to two hard jets and a photon remnant. The final term, $\sigma_{direct}^{\gamma p}$, is the 'direct photon' component and involves the direct scattering of the photon with a parton in the proton. Examples of this process are

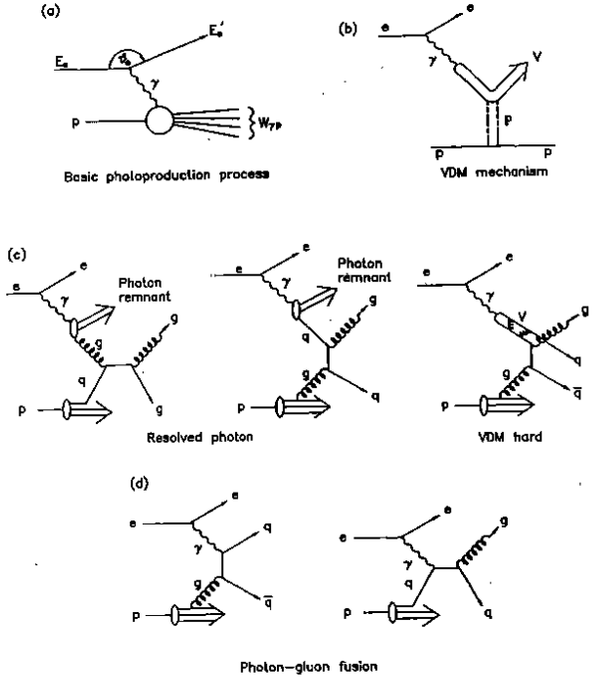

Figure 9: (a) The basic photoproduction diagram with a definition of the kinematic variables, (b) the vector dominance mechanism, (c) examples of the resolved photon process and (d) the photon - gluon fusion mechanism.

shown schematically in figure 9(d). The photon can interact with a quark in the proton (QCD Compton scattering) or with a gluon (boson-gluon fusion). This process gives rise to two hard jets of hadrons but with the absence of a photon remnant. One experimental task is to separate the direct and resolved photon processes from each other.

The extraction of the total γp cross section, based on 2 nb^{-1} of data, was one of the first physics measurement to be made at HERA [15, 16]. This involves an integration over the acceptance region which is dependent on the relative fractions of photoproduction processes. The main systematic uncertainty arises from the photon tagging efficiency and the acceptance of the main detector. From the 25 nb^{-1} sample of tagged events the values obtained from the two experiments are H1 : $\sigma_{tot}^{\gamma p}$=156±2±18 μb ($< W >$=197 GeV) and ZEUS : $\sigma_{tot}^{\gamma p}$=143±4±17 μb ($< W >$=180 GeV). These values are compared to those obtained in lower energy photoproduction experiments (up to W=18 GeV) [17] in figure 10. The solid curves are theoretical predictions; the curves labelled DL [18] and ALLM [19] are Regge-type analyses which have used the lower energy photoproduction measurements and photon structure function data to predict $\sigma_{tot}^{\gamma p}$ at higher energies. The other curves are based on QCD predictions of 'minijet' models which assume the total cross section is the sum of a soft part and a hard part [20]. Two values of p_T^{min} cut-off are compared with the data. It can be seen that the HERA measurements indicate that the γp total cross section does not rise dramatically with energy and that the Regge parameterizations are in better agreement with the data; the minijet models require choosing p_T^{min} to be 2.0 GeV or greater to be compatible with the data.

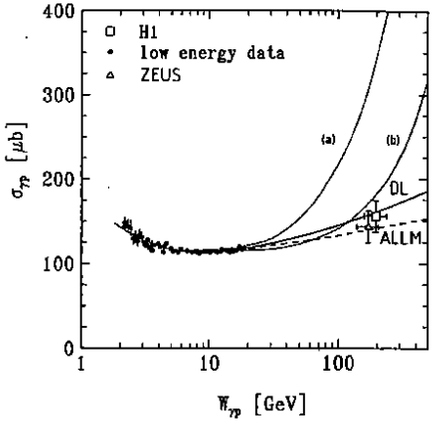

Figure 10: The total γp cross section measurements as a function of W. Theoretical comparisons (see text) are shown. The dotted lines show the minijet model with p_T^{min} cutoffs of (a) 1.4 GeV/c and (b) 2.0 GeV/c.

Using the tagged event sample, ZEUS has measured the relative contributions to $\sigma_{tot}^{\gamma p}$ from the various subprocesses, utilizing the angular dependence of calorimetric energy in photoproduction events [21]. The respective ratios contributing to $\sigma_{tot}^{\gamma p}$ are (10.5±0.6±3.7)% from vector meson production, (23.4±1.3±4.8)% from inelastic diffractive and (66.1±1.0±4.0)% from non-diffractive processes at $< W >\approx$180 GeV. The elastic diffractive process $ep \rightarrow e\rho^0 p$ has been directly observed by both experiments [21, 22]. Figure 11 shows an example of such an event in the H1 detector; two and only two tracks from the $\rho \rightarrow \pi^+\pi^-$ decay are seen in the detector with no evidence of a proton remnant in the forward direction, an indication of a purely diffractive process. H1 selects a two track sample with associated isolated calorimeter clusters in untagged photoproduction events. Figure 12 shows the effective mass of the two tracks in this sample, assigning each the pion mass. A clear ρ^0 peak is observed.

The presence of hard scattering in photoproduction has previously been observed at HERA [23, 24] and these processes are in marked contrast to the 'soft' processes described above. The hard processes are characterized in terms of resolved and direct photoproduction,

shown schematically in figure 9. A study of hard processes requires a search for jets in photoproduction events, either in the tagged sample (H1 and ZEUS) or the untagged sample (ZEUS). A calorimeter cluster is counted as a jet if the cluster radius in rapidity-azimuthal angle space satisfies the Snowmass convention [25], namely $R = \sqrt{\Delta\eta^2 + \Delta\phi^2} < 1$, and the cluster transverse energy, $E_T^{cluster}$, is greater than 7 GeV (H1) and 5 GeV (ZEUS). The jet rapidity can be computed for all such clusters. The incident photon energy can be determined for untagged events from longitudinal energy and momentum balance or for tagged events also from $E_\gamma = E_e - E_{e'}$. Candidate resolved and direct photoproduction events are shown in figure 13(a) and (b).

The H1 inclusive one-jet photoproduction cross section is shown as a function of jet E_T and rapidity in figure 14 [26]. An additional systematic error of 40% in the overall normalization has not been added to the data points. Note that jets extend out to an E_T of ~16 GeV. The data are compared to the Pythia Monte Carlo program [27] with a different set of photon structure functions [28]. Clearly the measurements are very sensitive to this photon structure. With the current 25 nb^{-1} data sample, the shape of the E_T distribution is well described by leading order QCD calculations. However, none of the models describe well the measured rapidity dependence. In order to pin down the favoured models more statistics will be required and the systematic errors reduced.

ZEUS have studied di-jet production by selecting events with two or more jets with the highest E_T in the rapidity range η^{jet} <1.6, leaving 284 events in the untagged sample [29]. The di-jet invariant

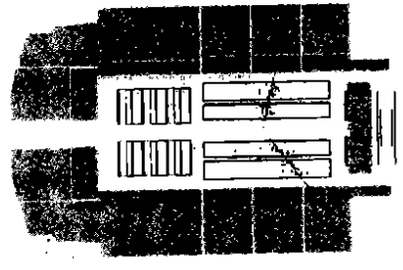

Figure 11: An elastic ρ event observed in the H1 detector.

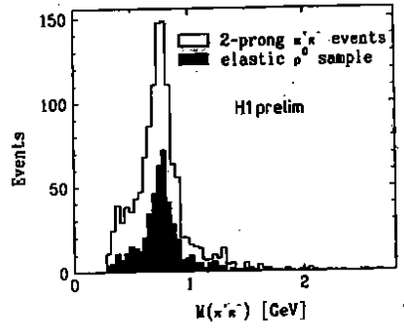

Figure 12: The two track $\pi^+\pi^-$ effective mass distribution measured in H1, showing a clear ρ peak.

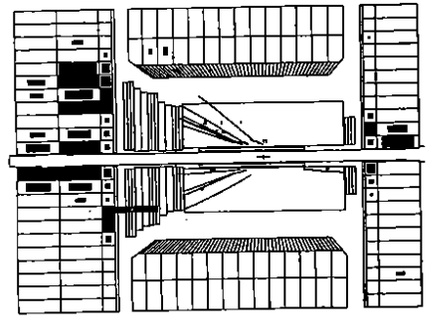

(a)

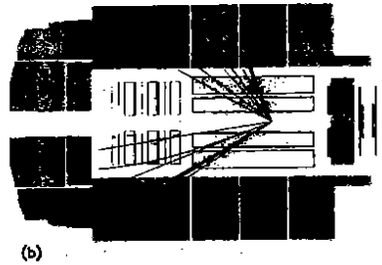

(b)

Figure 13: Candidate events : (a) a resolved photon event measured in ZEUS and (b) a direct photon event in H1.

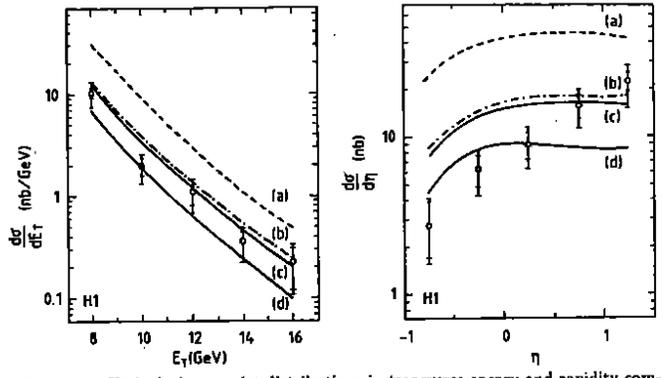

Figure 14: H1 inclusive one-jet distributions in transverse energy and rapidity compared to Monte Carlo predictions with different photon structure functions : (a) LAC-3, (b) LAC-2, (c) GRV-LO and (d) GRV-LO excluding the gluon.

mass distribution, m^{jj}, shown in figure 15(a), extends up to 40 GeV. The prediction of the Herwig Monte Carlo [30] (normalized to the data) is shown for comparison and is in good agreement; the relative contributions from resolved and direct photon contributions are indicated. The scattering angular distribution $\cos\theta^*$, where θ^* is calculated with respect to the incident proton direction (z axis) in the centre of mass frame of the two jets, is shown in figure 15(b) for $m^{jj} > 16$ GeV. This reflects the angular distributions of the parton-parton scattering processes and QCD predictions again agree with the data.

ZEUS has used their di-jet samples to separate the contributions from the direct and resolved photon processes. Figure 16(a) shows schematically the scattering of a parton (a quark or gluon) from the photon, labelled a, with a parton from the proton, labelled b. Assuming a low Q^2 (collinear) scattering process as depicted in figure 16(b), it can be shown that the fraction of the photon's momentum carried by parton a is given by $x_\gamma = \frac{E_a}{E_\gamma} = \frac{\Sigma(E-p_z)_{jets\ only}}{\Sigma(E-p_z)_{total\ calorimeter}}$. Here the numerator is the sum of the energy minus the third component of momentum, extending only over the two jet clusters; the denominator is the sum of $E - p_z$ over all calorimeter cells (ie over the complete event). Assuming the photon remnant is detected in the calorimeter, the quantity x_γ will give a value less than 1 for the resolved process and be equal to 1 for the direct process. Using this definition, the

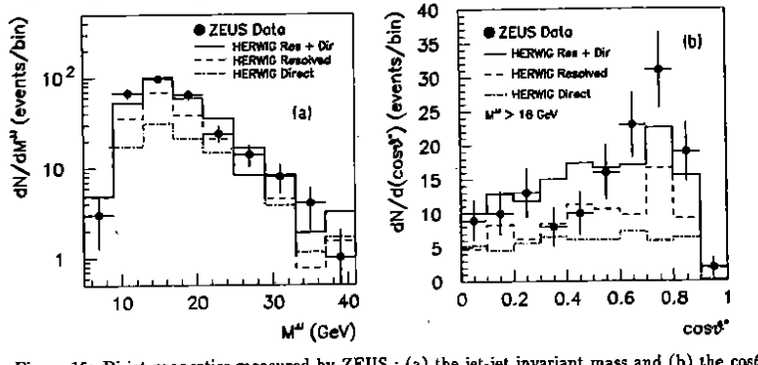

Figure 15: Di-jet properties measured by ZEUS : (a) the jet-jet invariant mass and (b) the $\cos\theta^*$ of jet angles.

distribution of x_γ measured in ZEUS is shown in figure 17(a). The Herwig Monte Carlo simulation, which breaks down the contributions from the subprocesses, is shown for comparison. The peak at high x_γ in the data cannot be described by the resolved photon process and therefore must result from direct processes. A similar peak is also observed in a sample of 44 tagged events.

An alternative method for evaluating x_γ is used by the H1 collaboration. H1 use tagged events and calculate the quantity $x_\gamma = \frac{E_T^{(1)} e^{-\eta_1} + E_T^{(2)} e^{-\eta_2}}{2yE_e}$ where $E_T^{(1)}$ and η_1 are the transverse energy and the rapidity of jet 1 (similarly for jet 2), y is the scaling variable defined in section 3 and E_e is the incident electron energy. Note that unlike the ZEUS definition of x_γ, everything is measured in the H1 analysis since tagged events are used; hence the measurement does not rely on the photon remnant being fully contained in the detector. The distribution of x_γ is shown in figure 17(b). The reason that the distribution looks very dissimilar from that of ZEUS is because the kinematic range is different and resolution effects smear out the peak at $x_\gamma \simeq 1$. An absolute Monte Carlo prediction incorporating the GS photon structure functions [28], with and without the gluon component of the photon, is shown for comparison. It can be seen that the measurement is sensitive to the gluon distribution in the photon.

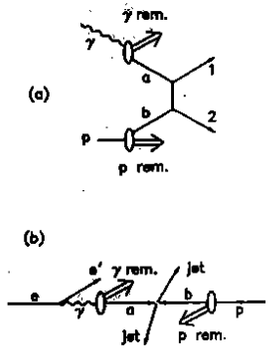

Figure 16: (a) Schematic of the γp interaction demonstrating (b) the collinearity of the scattering process.

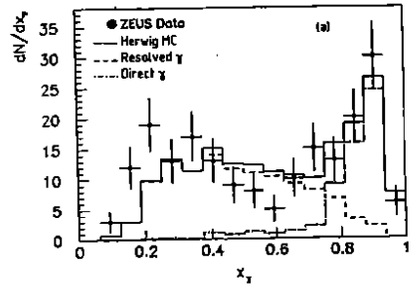

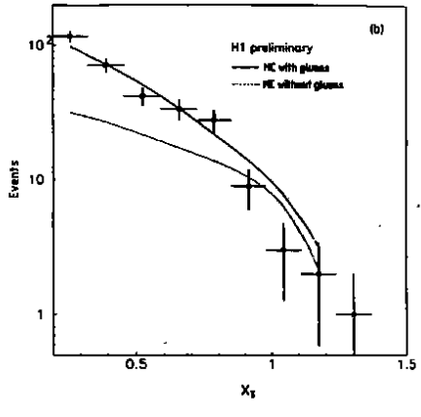

Figure 17: x_γ measured by (a) ZEUS and (b) H1.

4. Diffractive Events in DIS

The DIS mechanism for scattering an incident lepton from a (coloured) quark is shown in figure 18(a). The scattered remnant of the proton has net colour and hence there must be colour flow between the resulting di-quark and the struck quark (current jet). This results in the rapidity interval being populated with final state hadrons and hence DIS events

should have substantial energy deposits close to the proton beam direction. This is indeed observed [31, 32].

The H1 and ZEUS Collaborations both observe a class of DIS events where hadronic energy does not fill the space between the current jet and the proton beam direction [33, 34], a phenomenon not described by standard QCD inspired models. The x and Q^2 of these events extend from 10^{-4} to 10^{-2} and 4 to 100 GeV^2 respectively. Described in terms of pseudorapidity, $\eta = -\log_e(\tan\frac{\theta}{2})$ where θ is the polar angle with respect to the proton direction (positive z), these events have a sizeable difference between the rapidity of the smallest detector angle ($\theta \sim 1.5^0$, $\eta \sim 4.3$ for ZEUS and $\theta \sim 3.5^0$, $\eta \sim 3.5$ for H1) and the rapidity of hadrons observed closest to the incident proton direction. These so-called 'large rapidity gap' events are a very interesting new class of DIS.

A striking example of the difference between a rapidity gap event and a standard DIS event in ZEUS is shown in figure 19. For the former class, the lack of hadronic activity in the forward proton direction is apparent. Standard cuts are used to select the DIS sample but with a relaxation of the requirement of forward calorimeter energy $E_{FCAL} >$ 1 GeV [32, 34]. The quantity η_{max} is then defined as the maximum pseudorapidity of all calorimeter clusters in an event, where a cluster is defined as an isolated set of adjacent cells with summed energy greater than 400 MeV. The distribution of η_{max} is shown in figure 20. A DIS Monte Carlo simulation is shown for comparison. Note that a clear excess of events (78±10) is observed for $\eta_{max} < 1.5$ which corresponds to 5.4% of the total DIS sample (considered to be a lower limit due to acceptance effects). Note also that the distribution is flat below $\eta_{max} < 1.5$.

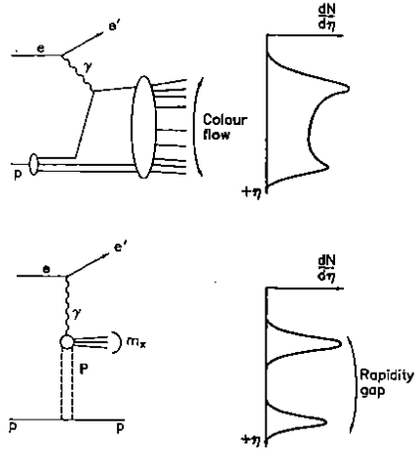

Figure 18: Schematic diagrams describing particle production and particle rapidity density (a) for standard DIS and (b) for diffractive dissociation in DIS.

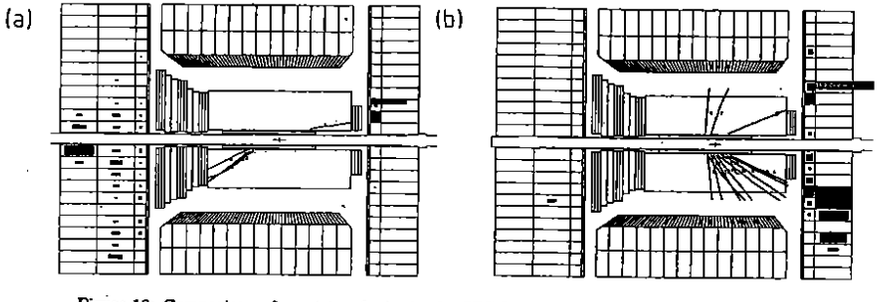

Figure 19: Comparison of event topologies in the ZEUS detector : (a) a typical DIS event and (b) an event with a large rapidity gap.

Rapidity gap events are also observed in H1 [33]. The difference in rapidity between the smallest detector angle and the rapidity of the hadron closest to the proton direction (again defined as a calorimeter cluster with energy greater than 400 MeV), $\Delta\eta$, is shown in figure 21. A clear excess of events over the Monte Carlo prediction is observed above $\Delta\eta > 2$, amounting to 6% of the DIS sample.

In the ZEUS analysis the DIS events are divided into two classes, one with $\eta_{max} < 1.5$ and the other with $\eta_{max} > 1.5$. Figure 22(a) shows the correlation between the invariant mass, m_X, of the observed hadronic system in the detector and the total centre of mass energy in the $\gamma^* p$ system, W. It can be seen that for $\eta_{max} < 1.5$, m_X is small compared to W, typically smaller than 10 GeV. The events are well separated from the rest of the sample for W >150 GeV. In figure 22(b) the ratio (r) of the number of DIS events with η_{max} <1.5 to the total number of DIS events is plotted as a function of W. Above 150 GeV the W distribution is consistent with being flat within errors. Figure 22(c) shows the distribution of m_X^2 for events with $\eta_{max} < 1.5$ and W >150 GeV, not corrected for detector resolution and acceptance effects. Given the statistical errors, the data are compatible with a $\frac{1}{m_X^2}$ dependence.

H1 and ZEUS have measured the quantity R, the ratio of the number of DIS events with $\Delta\eta$ >2 to the total number of DIS events. This is shown for H1 as a function of $\log(x)$ and Q^2 in figure 23. R is flat as a function of Q^2 and this implies that the production mechanism responsible for the large rapidity gap events shows a leading twist behaviour, ie the Q^2 distribution goes as $\frac{1}{Q^2}$ as in standard DIS.

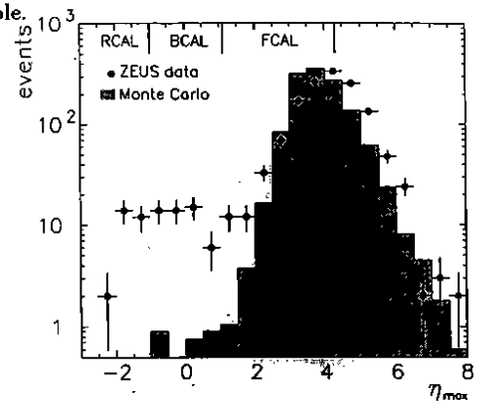

Figure 20: The distribution of η_{max} measured in ZEUS for data (points) and Monte Carlo (histogram).

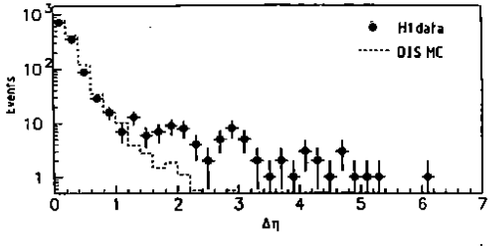

Figure 21: The distribution of $\Delta\eta$ measured in H1 for data (points) and Monte Carlo (histogram).

We come now to the interpretation of these events. The flat rapidity distribution, the lack of W dependence and the shape of the m_X^2 distribution suggest a diffractive interaction between a highly virtual photon and the proton, mediated by the exchange of a colourless object, the Pomeron [35]. The process is shown schematically in figure 18(b). This is the first observation of diffractive processes with large rapidity gaps in DIS, although the possibility of such a phenomenon has been previously suggested [36].

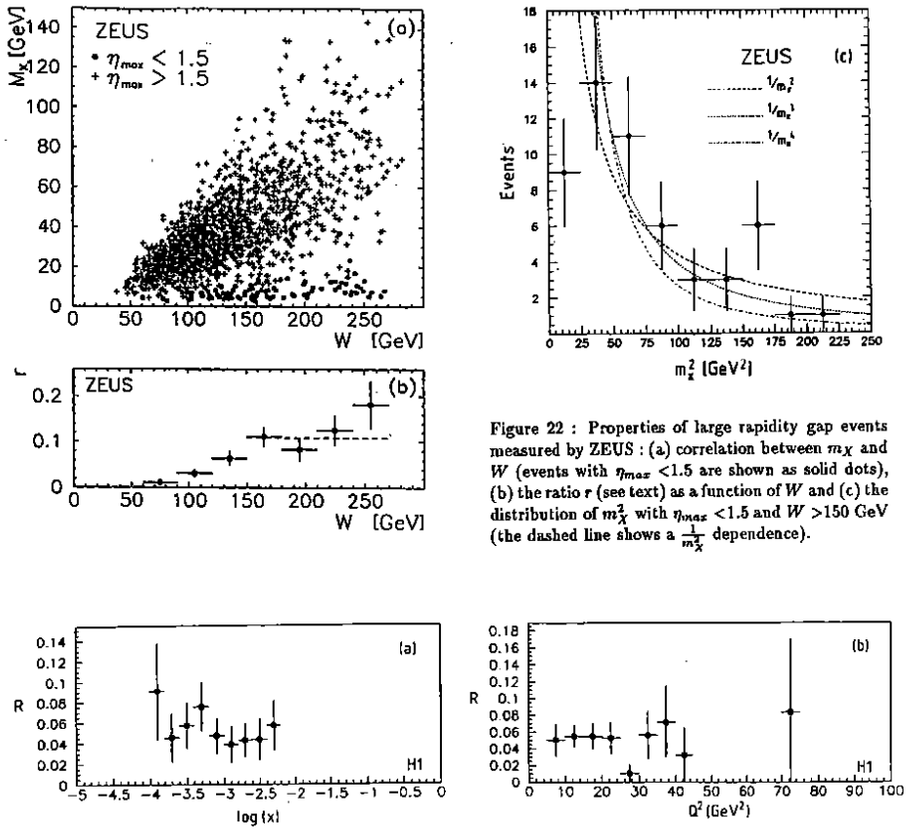

Figure 22 : Properties of large rapidity gap events measured by ZEUS : (a) correlation between m_X and W (events with η_{max} <1.5 are shown as solid dots), (b) the ratio r (see text) as a function of W and (c) the distribution of m_X^2 with η_{max} <1.5 and W >150 GeV (the dashed line shows a $\frac{1}{m_X^4}$ dependence).

Figure 23 : The ratio R (see text) measured in H1, (a) as a function of log(x) and (b) as a function of Q^2.

5. Summary

In summary, no evidence for the production of leptoquarks or leptogluons has been found at HERA and limits on the coupling strengths and masses have been derived. Soft and hard photoproduction processes have been studied and the γp total cross section has been determined. In hard photoproduction processes, direct and resolved photon interactions have been separated. In the DIS scattering at HERA, events have been observed with a large rapidity gap in the hadronic final state which have been interpreted as the diffractive dissociation of the highly virtual photon.

The experiments were made possible by the inventiveness and the diligent efforts of the H1 and ZEUS experimental teams and the HERA machine group. Useful and informative discussions with Drs. J.Butterworth, J.B.Dainton, G.Grindhammer, J.F.Martin, A.De Roeck, J.Whitmore and G.Wolf are gratefully appreciated.

References

[1] Technical Proposal for the H1 Detector (1986). H1 Collab., I.Abt et al., DESY 93-103. Submitted to Nucl. Inst. and Meth.

[2] The ZEUS Detector, Technical Proposal (1986). D.H. Saxon, Proc. of the 1987 HERA Workshop, DESY, Hamburg (Oct 1987). Vol.2 903.

[3] G.Grindhammer. $F_2^p(x,Q^2)$ and the Hadronic Final State in DIS. These proceedings.

[4] J.C.Pati and A.Salam, Phys. Rev. D10 (1974) 275. H.Georgi and S.Glashow, Phys. Rev. Lett. 32 (1974) 438. J.L.Hewett and T.G.Rizzo, Phys. Rep. 183 (1989) 193. R.J.Cashmore et al., Phys. Rep. 122 (1985) 275. W.Buchmüller, Schladming Lectures Suppl. XXVII (1985) 517. And references therein.

[5] OPAL Collab., M.Akrawy et al., Phys. Lett. B263 (1991) 123. L3 Collab., B.Adeva et al., Phys. Lett. B261 (1991) 169. DELPHI Collab., P.Abreu et al., Phys. Lett. B275 (1991) 222. ALEPH Collab., D.Decamp et al., Phys. Rep 216 (1992) 253.

[6] CDF Collab., S.Moulding et al., presented at the 7th Meeting of the APS, Fermilab, (Nov 1992). D0 Collab., J.T.White, 'Search for Supersymmetry and Leptoquark States in D0', these proceedings.

[7] H.Fritzsch and G.Mandelbaum, Phys. Lett. B102 (1981) 319. U.Baur and K.H.Streng Z. Phys. C30 (1986) 325.

[8] W.Buchmüller et al., Phys. Lett. B191 (1987) 442.

[9] H1 Collab., I.Abt et al., Nucl. Phys B396 (1993) 3.

[10] ZEUS Collab., M.Derrick et al., Phys. Lett. B306 (1993) 173.

[11] J.Bijnens, Proc. of the 1987 HERA Workshop, DESY, Hamburg (Oct 1987). Vol.2 819.

[12] K.Hagiwara et al., Z. Phys. C29 (1985) 115. F.Boudjema et al., Z. Phys. C57 (1993) 425.

[13] OPAL Collab., M.Akrawy et al., Phys. Lett. B257 (1991) 531. L3 Collab., B.Adriani et al., Phys. Lett. B288 (1992) 404. DELPHI Collab., P.Abreu et al., Z. Phys. C53 (1992) 41. ALEPH Collab., D.Decamp et al., Phys. Rep 216 (1992) 253.

[14] ZEUS Collab., M.Derrick et al., Phys. Lett. B316 (1993) 207.

[15] H1 Collab., T.Ahmed et al., Phys. Lett. B299 (1993) 374.

[16] ZEUS Collab., M.Derrick et al., Phys. Lett. B293 (1992) 465.

[17] S.I.Alekhin et al.,CERN-HERA 87-01 (1987) and references therein.

[18] A.Donnachie and P.V.Landshoff, Nucl. Phys. B244 (1984) 322.

[19] H.Abramowicz et al., Phys. Lett B269 (1991) 465.

[20] M.Drees and K.Grassie, Z. Phys. C28 (1985) 451. M.Drees and F.Halzen, Phys. Rev. Lett. 61 (1988) 275.

[21] 'Total and Partial Cross sections measured with the ZEUS detector at $\sqrt{s}$=180 GeV'. Paper in preparation.

[22] M.Erdmann et al., presented at the XXVIIth Recontres de Moriond, Les Arcs, March 1993. DESY 93-077.

[23] H1 Collab., A.Ahmed et al., Phys. Lett. B297 (1992) 205.

[24] ZEUS Collab., M.Derrick et al., Phys. Lett. B297 (1992) 404.

[25] J.Huth et al., Proc. of the 1990 DPF Summer Study on High Energy Physics, Snowmass, Colorado. Edited by E.L.Berger (World Scientific, Singapore, 1992) 134.

[26] H1 Collab., I.Abt et al., Phys. Lett. B314 (1993) 436.

[27] H.-U Bengtsson and T.Sjöstrand, Comp. Phys. Comm. 46 (1987). T.Sjöstrand, CERN TH6488/92.

[28] LAC-2, LAC-3 : Abramowicz et al., Phys. Lett. B269 (1991) 458. GRV-LO : M.Glück et al., Phys. Rev. D46 (1992) 1973. GS : L.E.Gorden and J.K.Storrow, Phys. Lett. B291 (1992) 320.

[29] ZEUS Collab., 'Observation of Direct Processes in Photoproduction at HERA'. DESY 93-151. Accepted by Phys. Rev. Lett.

[30] G.Marchesini et al.,Comp. Phys. Comm. 67 (1991) 465.

[31] H1 Collab., T.Ahmed et al., Phys. Lett. B298 (1993) 469. H1 Collab., I.Abt et al., Nucl. Phys. B407 (1993) 515.

[32] ZEUS Collab., M.Derrick et al., Z. Phys C59 (1993) 231. ZEUS Collab., M.Derrick et al., Phys. Lett. B316 (1993) 412.

[33] H1 Collab., 'Results from the H1 Experiment at HERA', invited talk presented by A. De Roeck at the International Europhysics Conference on High Energy Physics, Marseilles, France, July 1993. H1 Collab., 'Results from the H1 Experiment at HERA', invited talk presented by J.B. Dainton at the XVI International Lepton Photon Symposium, Cornell University, Ithaca, USA, August 1993.

[34] ZEUS Collab., M.Derrick et al., Phys. Lett. B315 (1993) 481.

[35] R.D.Field and C.G.Fox, Nucl. Phys. B80 (1974) 367. A.Donnachie and P.V.Landshoff, Nucl. Phys B231 (1984) 189. K.Goulianos, Phys. Rep. 101 (1983) 169.

[36] G.Ingelman and P.E.Schlein, Phys. Lett. B152 (1985) 256.